Article

Fault Detection of Landing Gear Retraction/Extension Hydraulic System Based on Bond Graph-linear Fractional Transformation Technique and Interval Analytic Redundancy Relations

Yuyuan Cao*,†, Shixuan Duan†, Yanjun Li, Xudong Li, Zejian Zhao and Xingye Wang

College of Civil Aviation, Nanjing University of Aeronautics and Astronautics, Nanjing 210016, China; caoyuyuan@nuaa.edu.cn (Y.C.); a1060586733@nuaa.edu.cn (S.D.); lyj@nuaa.edu.cn (Y.L.); lixudong@nuaa.edu.cn (X.L.); nuaazzj2020@nuaa.edu.cn (Z.Z.); nuaawxy@163.com (X.W.)

* Correspondence: caoyuyuan@nuaa.edu.cn

† Co-first author.

Featured Application: In the research on fault detection of landing gear retraction/extension hydraulic system, bond graph linear fractional transformation technology and interval analysis theory are applied to consider the uncertain negative factors in the system, thereby improving the accuracy and sensitivity.

Abstract: Various factors, such as uncertainty of component parameters and uncertainty of sensor measurement values, contribute to the difficulty of fault detection in the landing gear retraction/extension hydraulic system. In this paper, we introduce linear fractional transformation technology and uncertainty analysis theory for the construction of the diagnostic bond graph of the landing gear retraction/extension hydraulic system. In this way, interval analytical redundancy relations and fault signature matrix can be derived. Using the fault signature matrix, existing faults of the system can be preliminarily detected and isolated. Additionally, interval analytical redundancy relations can be used to detect system faults in detail, and cases analysis can be carried out to determine if the actuator is externally or internally leaky, and if the landing gear selector valve is reversing stuck. Compared to the traditional analytical redundancy relations, this method takes into account the negative factors of uncertainty; and compared to the traditional absolute diagnostic threshold, the interval diagnostic threshold is more accurate and sensitive.

Keywords: fault detection; retraction/extension (R/E) hydraulic system; bond graph-linear fractional transformation technique; interval analytic redundancy relations; uncertainty; fault signature matrix; residuals; thresholds

1. Introduction

Boeing, Airbus, EASA (European Union Aviation Safety Agency), and ICAO (International Civil Aviation Organization) [1-4] report more than 50% of fatal accidents occur during final approach and landing phases. Landing gear performance is directly related to aircraft takeoffs and landings due to its irreplaceability. To accomplish retraction/extension of the landing gear, the retraction/extension (R/E) hydraulic system is the key subsystem. In order to ensure takeoff and landing safety, fault diagnosis of landing gear R/E hydraulic systems is crucial. However, fault detection is the first step in fault diagnosis.

Research methods for fault diagnosis of complex nonlinear systems such as hydraulic systems fall into three categories: knowledge-based, data-driven, and model-based [5]. In knowledge-based methods, knowledge reasoning and long-term accumulated experience knowledge are mainly used [6-8]. In data-driven analysis, a large amount of online and offline data from the system is analyzed [9-13]. Based on a model-based approach, this

 doi:10.20944/preprints202207.0247.v2

paper examines whether there is a consistency criterion between the system's actual output and its expected output. State estimation methods, parameter estimation methods, and equivalent space methods are kinds of model-based methods.

Generally, state estimation methods compare the state output of the system model with the output of the actual system to generate system residuals that are used as consistency criteria. Observer and filter methods are used, with Kalman filter being the most commonly used. Most of the studied systems are nonlinear systems, which are inevitably affected by various factors such as the uncertainty of model parameters, the interaction between components and systems, the interaction between environment and systems, and noise. Therefore, most experts and scholars mainly focus on the robust state estimation of nonlinear systems. In the research of observer method, Hu Zhenggao [14] proposed nonlinear adaptive unknown input observer, Liu Yingming [15] realized sliding mode control of rolling mill using disturbance observer, and Xu Guosheng [16] realized sliding mode control of excavator based on high-gain observer. In the research of Kalman filter, various improved Kalman filters or their variants have been produced, such as extended Kalman filter [17], multiple outlier robust Kalman filter [18], federated Kalman filter [19], unscented Kalman filter [20], distributed Kalman filter [21], etc.

In parameter estimation method, the estimated physical parameters are compared with the nominal values in order to generate the system residual. This serves as a consistency criterion for the core idea. There are two common estimation methods: joint estimation and minimum error estimation. In the joint estimation method [22,23], the estimated parameters are used as the extension of the state, and the state estimation method is used to estimate the state and parameter. Despite its simplicity and speed, this method may result in dimension disaster if the space dimension is too high after expansion. Compared to the extended state space method, the method based on multi structure observer and filter [24] has stronger robustness and lower computational difficulty. Further, the minimum error method [25] is mostly used for off-line fault diagnosis, and its accuracy depends on the completeness of data samples.

Core principle of equivalent space method is to use the residual between input and output of the analytical model of the system as a consistency criterion. Using hardware redundancy, multiple redundant sensors are set up and residuals are derived from the measurement model for analysis. Although this method is simple and easy, it also requires multiple redundant sensors, so its cost is high. As a consistency criterion of the core diagnosis idea, an analytical redundancy relations (ARRs) method builds the residual indirectly through an analytical mathematical model. Using power bond graph and relying on the energy conservation law, this method has some drawbacks, including parameter uncertainty, sensor measurement uncertainty, environmental impact, and noise. As a result, the residual generated by the system will fluctuate, leading to misdiagnosis and missed diagnoses. It is necessary to incorporate system uncertainty robustness into the bond graph model to improve this problem. Bond graph-linear fractional transformation (BG-LFT) is the most effective solution to this problem. On the basis of this technology, Mo Haobin [26] proposed a fault diagnosis method based on interval analytical redundancy relationships in order to avoid the interference of system uncertainty on diagnosis results. Wang Fang [27] designed a robust diagnosis observer for hybrid systems, and combined BG-LFT and proportional integrator to realize robust fault diagnosis and estimation, which improved the detection effect. M.A. Djeziri [28] believes that all uncertainties are cumulative in the diagnosis threshold of node residual. In this way, uncertainty interaction will be ignored, which may lead to overestimation of the diagnosis threshold.

Previous literature [29] published by us focuses mainly on evaluating failed systems, which belongs to the belongs to the research after fault detection. In this paper, we focus on the problems in the process of fault detection and make the following contributions:

- By combining bond graph linear fractional transformation technology and interval analysis theory, the diagnostic modeling of uncertain interference factors landing gear R/E hydraulic system is carried out.

Preprints (www.preprints.org) | NOT PEER-REVIEWED | Posted: 17 August 2022 doi:10.20944/preprints202207.0247.v2

- Using the fault signature matrix (FSM), the relevant landing gear R/E hydraulic fault parameters are preliminarily detected and isolated.
- According to the analysis of fault cases, the proposed asymmetric interval threshold has better detection accuracy and sensitivity than the traditional absolute threshold.

This paper is structured as follows:

Section 1: A brief review of the research areas related to model-based fault diagnosis.

Section 2: Landing gear R/E hydraulic system is modeled using power bond graph.

Section 3: Modeling of uncertainty diagnosis bond graph of landing gear R/E hydraulic system based on bond graph-linear fractional transformation technology and interval analytical redundancy relations. .

Section 4: Study on residuals and its uncertainty.

Section 5: Case analysis of the external and internal leakage of actuator and the stuck reversing of the landing gear selector valve.

Section 6: Conclusion and prospect.

2. Overview of landing gear retraction/extension hydraulic system and its traditional diagnosis bond graph

2.1. Basic system framework

Figure 1 depicts the basic framework of the landing gear retraction/extension (R/E) hydraulic system. Power is provided by both an electric motor-driven pump and an engine-driven pump, and combine with other accessories to form a hydraulic source. High pressure hydraulic oil is distributed to the R/E hydraulic components of the left and right MLG (main landing gear) and NLG (nose landing gear) by the hydraulic components of the landing gear selector valve. Figure 1 only shows the most important parts of the function, and does not show accessories such as check valve, throttle valve and hydraulic fuse.

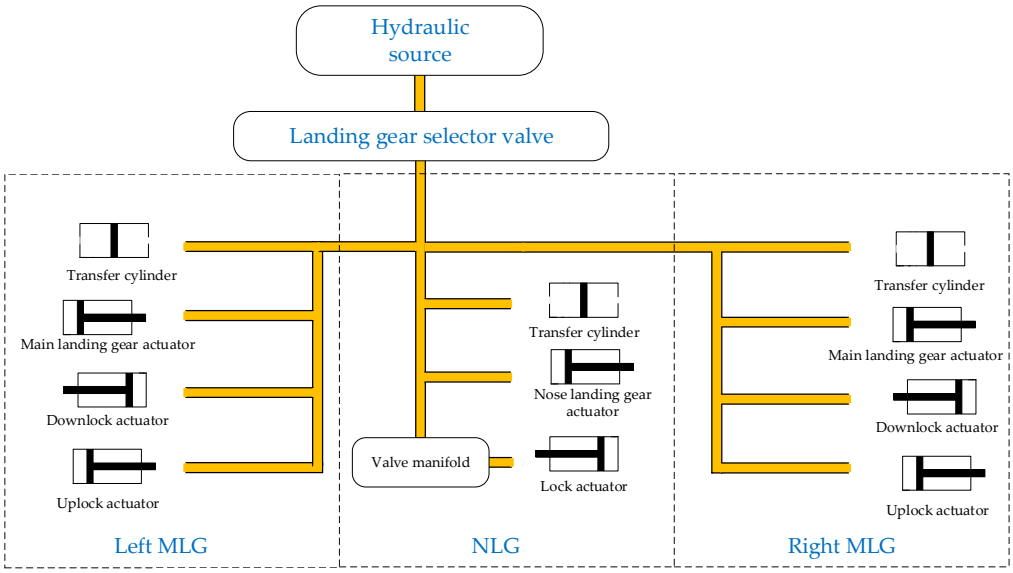

Figure 1. Basic structure of landing gear R/E hydraulic system.

In the subsequent bond graph modeling, where the generalized potential variable e in the hydraulic system refers to the pressure p, and the generalized flow variable f refers to the flow rate Q [30]. All models must satisfy the fundamental requirements of equal pressure at the common potential node (0-node) and equal flow at the common flow node (1-node). State and variation quantities of pressure are located on the half-tip arrow's side, whereas state and variation quantities of flow are located on the side without the tip. The signal bond is indicated by the entire arrow, which denotes that there is a functional connection between the parametric parameters at its two endpoints.

Preprints (www.preprints.org) | NOT PEER-REVIEWED | Posted: 17 August 2022 doi:10.20944/preprints202207.0247.v2

2.2. Modeling of landing gear selector valve

Figure 2(a) illustrates the physical essence of the landing gear selector valve, which is a Y-type, 3-position 4-way solenoid directional valve. The P-port closed A, B, and T ports connected, the floating piston, ability to move in response to external forces, and hydraulic pump does not unload are the characteristics that define its median function. Figures 2(b) (c) (d) depict the landing gear selector valve's neutral, left, and right operational states. Figure 3 depicts the bond graph model of the landing gear selector valve.

Port P is the supply port, Port T is the return port, and Ports A and B are connected to the subsequent pipes. 4 paths (PA, PB, AT, BT) are formed by the valve body and spool's relative positions, and the corresponding fluid resistance are R_{PA}, R_{PB}, R_{AT}, and R_{BT}.

Neutral, left, and right working states have the following meanings [31]:

1) Neutral: Now that the high pressure source P port is disconnected from the system, A and B ports are attached to the return port T. Hydraulic oil returns to the tank through the hydraulic resistance R_{AT} of the AT path and the hydraulic resistance R_{BT} of the BT path, respectively. At this time, liquid resistance R_{PA} and R_{PB} are not considered.

2) Left: Port A is connected to the return port T, whereas port B is connected to the high pressure source port P. Through R_{PB} of the PB path, high pressure hydraulic oil exits from port B. Through R_{AT} of the path AT, hydraulic oil from the return line flows back to tank. Liquid resistance R_{PA} and R_{BT} are not taken into consideration at this time.

3) Right: Port B is connected to the return port T, whereas port A is connected to the high pressure source port P. Through R_{PA} of the PA path, high pressure hydraulic oil exits from port A. Through R_{BT} of the path BT, hydraulic oil from the return line flows back to tank. Liquid resistance R_{PB} and R_{AT} are not taken into consideration at this time.

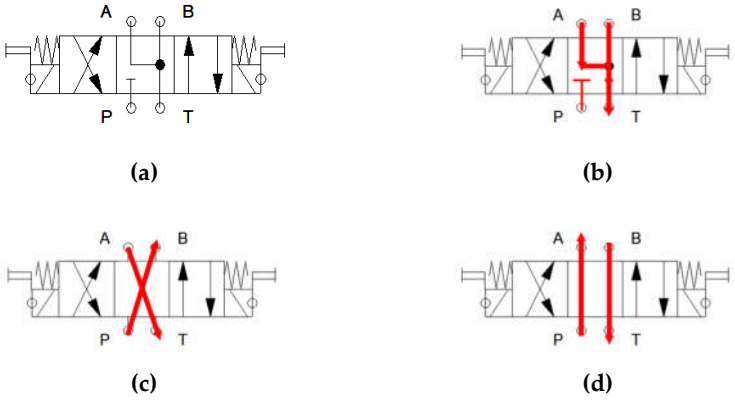

Figure 2. Landing gear selector valve and its working state: (**a**) Landing gear selector valve; (**b**) Neutral function; (**c**) Left position status; (**d**) Right position status.

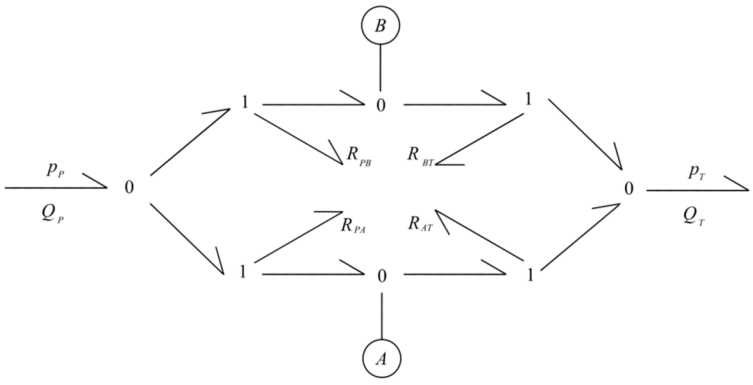

Figure 3. Landing gear selector valve bond graph.

Preprints (www.preprints.org) | NOT PEER-REVIEWED | Posted: 17 August 2022 doi:10.20944/preprints202207.0247.v2

2.3. Modeling of actuator

Actuator is a component used to reciprocate linear motion in a hydraulic system by converting hydraulic energy into mechanical energy. Landing gear R/E hydraulics include the main landing gear actuator, downlock actuator, uplock actuator, and nose landing gear actuator and lock actuator [32].Transfer cylinder can be regarded as an actuator with a diameter of 0 on both sides of the piston rod. Since all actuators have the exact same physical characteristics, only one modeling is needed. Although there are many actuators in the system, by only using the R/E actuator as terminals, the analysis is made simpler. The model is depicted in Figure 4, and Table 1 lists the definitions of the parameters for the actuators.

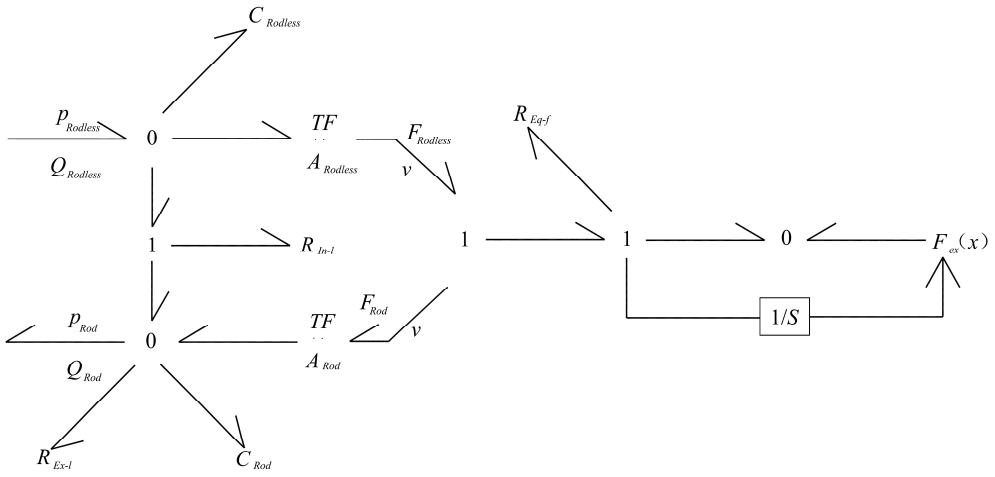

Figure 4. Actuator bond graph.

Table 1. Parameters definition of actuators bond graph.

Parameter name	Meaning
$p_{Rodless}$ $Q_{Rodless}$	Pressure and flow of rodless cavity
p_{Rod} Q_{Rod}	Pressure and flow of rod cavity
$A_{Rodless}$ $F_{Rodless}$	Acting area and force of piston on one side of rodless cavity
A_{Rod} F_{Rod}	Acting area and force of piston on one side with rod cavity
v	Piston velocity
R_{Ex-l}	Hydraulic resistance effect of external leakage of actuator
$C_{Ex-Rodless}$ C_{Ex-Rod}	Liquid capacity effect of rodless cavity and rodless cavity
R_{In-l}	Hydraulic resistance effect of internal leakage of actuator
R_{Eq-f}	Equivalent friction liquid resistance effect of reciprocating motion outside the actuator
$F_{ex}(x)$	Other external forces acting on external loads

2.4. Modeling rules and diagnostic bond graph

The system traditional diagnostic bond graph is shown in Figure 5. According to the literature [33], the following guidelines were used to determine the causal relationship:

- There is a sole causal relationship between the potential source and the flow source, with the potential source's causality stroke on the side closest to the tip and the flow source's causality stroke on the side farther from the tip.
- Both inertial and capacitive elements have precedence for defining integral causality, but the causality of the inertial element is on the side closest to the tip, whereas the causality of the capacitive element is on the side farthest from the tip.
- The resistive component prioritizes admittance type causality; the causality stroke is on the tip side, but coordination with other bond graph parts must be taken into

Preprints (www.preprints.org) | NOT PEER-REVIEWED | Posted: 17 August 2022 doi:10.20944/preprints202207.0247.v2

account throughout the designation process, and the causality is extended in the direction of flow at the node.

Each bond and node is numbered according to the following principles:

- Starting from number 1, each bond is numbered in turn, counterclockwise, centered on the node, and the signal bonds are not numbered.
- Starting from number *(1)*, each node is numbered according to the direction of energy flow, and the converter *TF* node is not numbered.

In Figure 5, the pre-defined fault nodes and the nodes where multiple bonds converge in the system are chosen as the virtual sensor placement locations. To detect the pressure signal, the pressure sensor *SSp* is placed at the common potential node (0-node), and to detect the flow signal, the flow sensor *SSQ* is placed at the common flow node (1-node). Table 2 displays the correspondence between the sensor's and analytical redundancy relations (ARRs).

Table 2. Set virtual sensors and corresponding ARRs.

Pressure virtual sensor	Flow virtual sensor
SSp_1 and SSp_3 : ARR_1	SSQ_1 : ARR_3
SSp_2 and SSp_4 : ARR_2	SSQ_2 : ARR_4

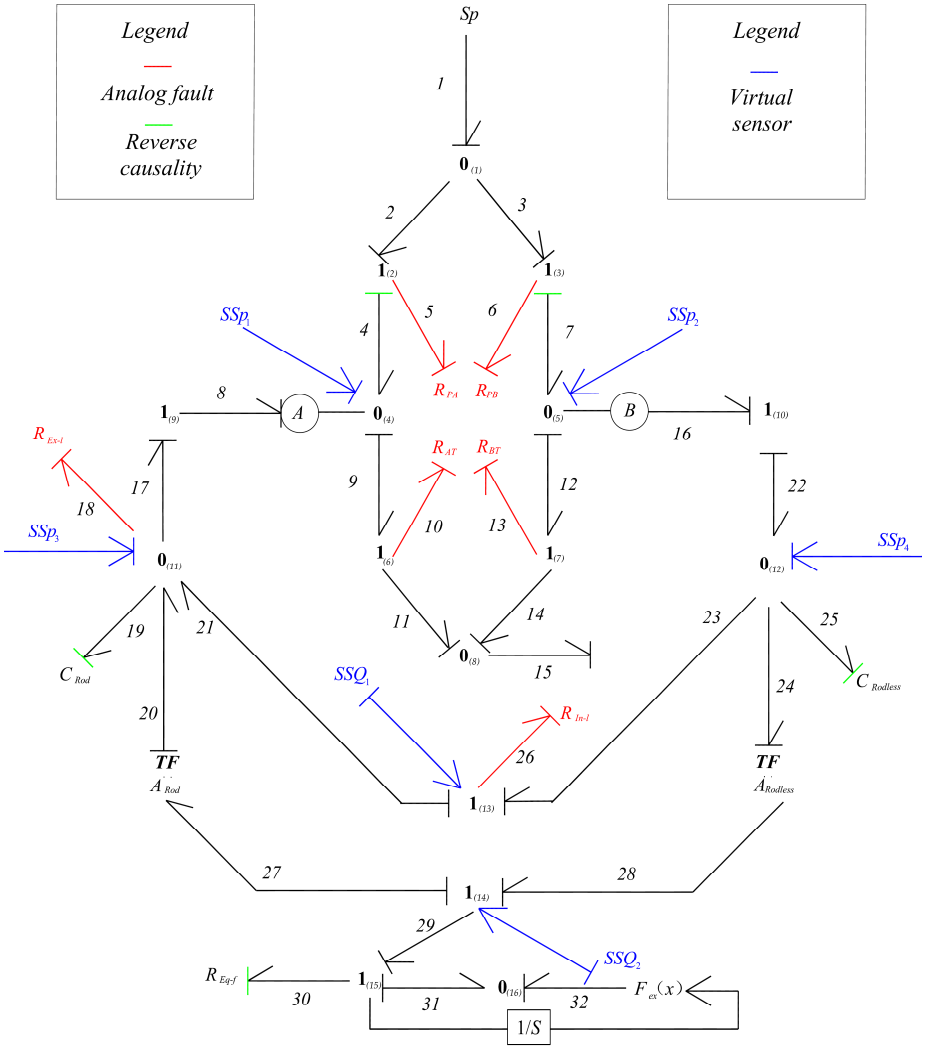

Figure 5. Traditional diagnostic bond graph of landing gear R/E hydraulic system.

Preprints (www.preprints.org) | NOT PEER-REVIEWED | Posted: 17 August 2022 doi:10.20944/preprints202207.0247.v2

3. Modeling method considering uncertainty

3.1. Uncertainty modeling of component parameters

Bond graph-linear fractional transformation technique (BG-LFT) [34] is a widely used and effective method for research considering system uncertainty. Figure 6 is a general model of the method.

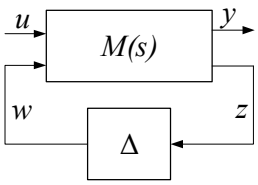

Figure 6. General model of BG-LFT.

In figure 6, $M(s)$ is an incidence matrix; Δ is the parameter uncertainty deviation matrix; u and y are actual input and output vectors, respectively; w and z are auxiliary input and output vectors, respectively.

Under the premise of not changing the causality of the original bond graph model, the uncertainty is expanded. Let the true values of the resistive element R, capacitive element C and inertial element I of the bond graph model be $\theta \in \{R, C, I\}$, the nominal value be $\theta_n \in \{R_n, C_n, I_n\}$ and the uncertainty value be $\theta \in \{\Delta R, \Delta C, \Delta I\}$.Then each value satisfies:

$$\theta = \theta_n + \Delta\theta \tag{1}$$

Define $\delta = \Delta\theta/\theta$ as relative uncertainty. Taking the resistive element as an example, specifically expressed as follows:

$$\begin{cases} \text{Impedance type}: p_R = Q_R R = Q_R(R_\theta + \Delta R) = Q_R R_\theta(1+\delta_R) = p_{R_n} + p_{\Delta R} \\ \text{Admittance type}: Q_R = \dfrac{p_R}{R} = \dfrac{p_R}{R_\theta + \Delta R} = \dfrac{p_R}{R_n}(1 - \dfrac{\Delta R}{R_n + \Delta R}) = Q_{R_n} + Q_{\Delta R} \end{cases} \tag{2}$$

Where, p_R is the actual output pressure, Q_R is the actual input flow, p_{R_n} is the nominal pressure of the element, and $p_{\Delta R}$ is the uncertainty pressure. The resulting image is shown in Figure 7. BG-LFT models of capacitive elements and inertial elements can be obtained by the same method, as shown in Figure 8 and Figure 9. Where $Dp*$ and $DQ*$ are sensor virtual pressure source and flow source respectively.

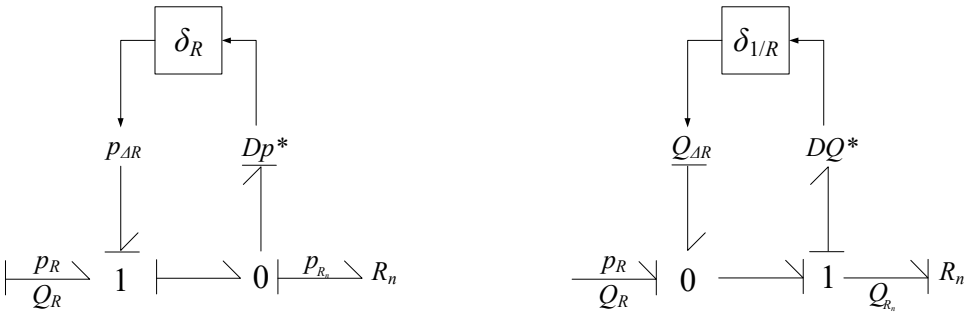

(a) **(b)**

Figure 7. BG-LFT model of resistive element: (a) Impedance type; (**b**) Admittance type.

Preprints (www.preprints.org) | NOT PEER-REVIEWED | Posted: 17 August 2022 doi:10.20944/preprints202207.0247.v2

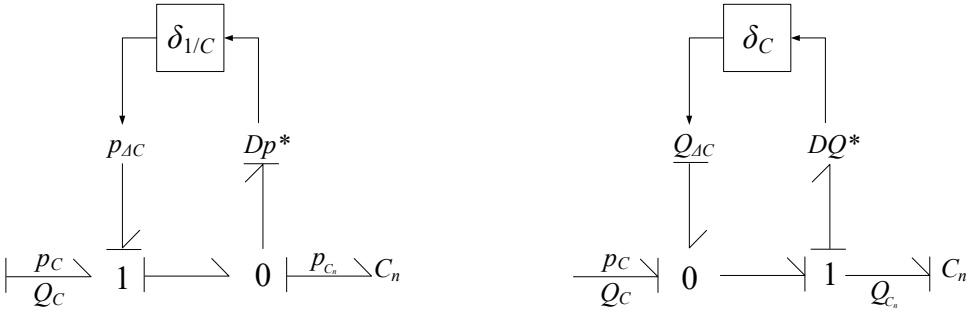

(a) **(b)**

Figure 8. BG-LFT model of capacitive element: (**a**) Integral type; (**b**) Differential type.

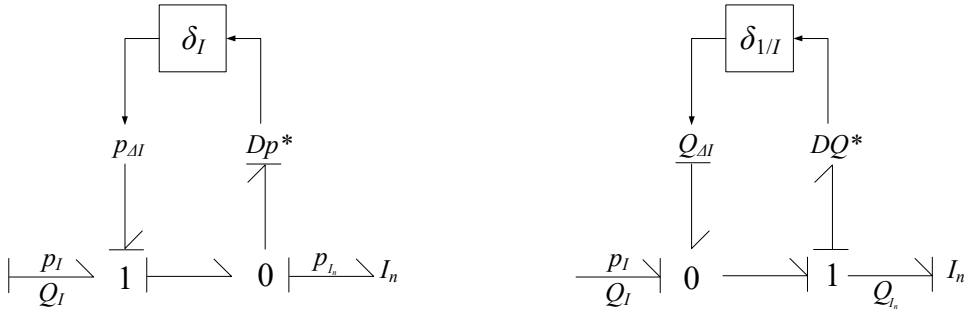

(a) **(b)**

Figure 9. BG-LFT model of inertial element: (a) Integral type; (**b**) Differential type.

3.2. Uncertainty modeling of sensor measurement

Due to the negative factors such as environmental impact and noise, the measured value of the sensor is often not the true value, and there is inevitable error [35,36]. Let the true value of the sensor be $S_T \in \{SSp_T, SSQ_T\}$, the measured value be $S_M \in \{SSp_M, SSQ_M\}$, and the measurement error be $\Delta S \in \{\zeta_{SSp}, \zeta_{SSQ}\}$. They have the following relationships:

$$S_T = S_M + \Delta S \tag{3}$$

Specific modeling of 0-node a is as follows:

Figure 10 (a) is a model without consideration of measurement uncertainty, and Figure 10 (b) is a model with consideration of measurement uncertainty.

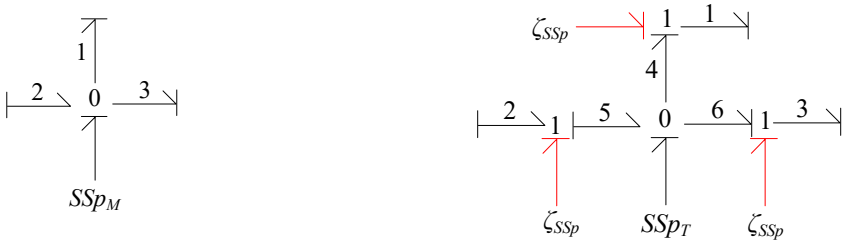

(a) **(b)**

Figure 10. Uncertainty model of pressure sensor measurement: (a) Not considered; (**b**) Considered.

Therefore, considering the uncertainty of the measured value of the sensor, its true value is:

Preprints (www.preprints.org) | NOT PEER-REVIEWED | Posted: 17 August 2022 doi:10.20944/preprints202207.0247.v2

$$\begin{cases} p_1 = p_2 = p_3 = SSp_M \\ p_1 = p_4 + \xi_{SSp} = SSp_M + \xi_{SSp} \\ p_2 = p_5 + \xi_{SSp} = SSp_M + \xi_{SSp} \\ p_3 = p_6 + \xi_{SSp} = SSp_M + \xi_{SSp} \end{cases} \tag{4}$$

Specific modeling of 1-node a is as follows:

Figure 11 (a) is a model without consideration of measurement uncertainty, and Figure 11 (b) is a model with consideration of measurement uncertainty.

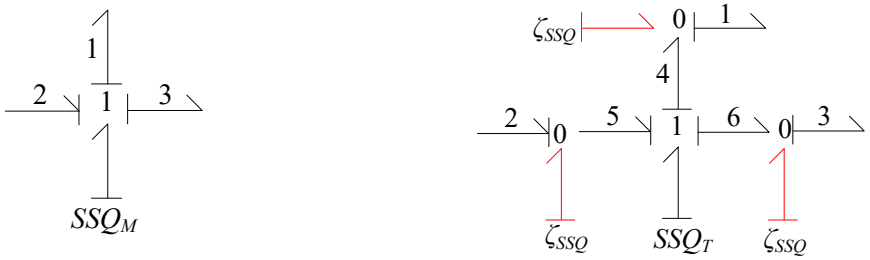

(a) **(b)**

Figure 11. Uncertainty model of flow sensor measurement: (a) Not considered; (**b**) Considered.

Therefore, considering the uncertainty of the measured value of the sensor, its true value is:

$$\begin{cases} Q_1 = Q_2 = Q_3 = SSQ_M \\ Q_1 = Q_4 + \xi_{SSQ} = SSQ_M + \xi_{SSQ} \\ Q_2 = Q_5 + \xi_{SSQ} = SSQ_M + \xi_{SSQ} \\ Q_3 = Q_6 + \xi_{SSQ} = SSQ_M + \xi_{SSQ} \end{cases} \tag{5}$$

3.3. Model extension based on interval analytic redundancy

Taking the resistive element as an example, for any pressure variable p:

$$p = (R_n + \Delta R)(SSQ_M + \zeta_{SSQ}) = R_n SSQ_M + [(R_n + \Delta R)\zeta_{SSQ} + \Delta R \cdot SSQ_M] \tag{6}$$

Therefore, $p_u = [(R_n + \Delta R)\zeta_{SSQ} + \Delta R \cdot SSQ_M]$ is defined as an uncertainty term. And $R_n SSQ_M$ is the residual term without considering the uncertainty.

Traditional analytical redundancy relations (ARRs) [37] are a constraint relationship obtained from a system model based on energy conservation rules.

$$\begin{cases} \mathrm{ARR}_i = f_i(k_i, \theta_i) \qquad i = 1, \cdots, n \\ \mathrm{ARRs} = [\mathrm{ARR}_1, \mathrm{ARR}_2, \cdots, \mathrm{ARR}_n] \\ r_i = \mathrm{ARR}_i = 0 \end{cases} \tag{7}$$

where i is the number of the ARR, k_i is the system variable, θ_i is the system parameter, and f_i is a function of the k_i and θ_i. r_i is the residual generated by the system node.

After introducing the theory of interval analytic redundancy, the traditional analytic redundancy is extended. $[\delta_\theta] = [-\Delta\theta_l/\theta_n, \Delta\theta_r/\theta_n]$ is defined as the relative uncertainty of parameter interval. For parameter uncertainty:

$$\left[\underline{\theta}, \overline{\theta}\right] = [\theta_n - \Delta\theta_l, \theta_n + \Delta\theta_r] = \theta_n(1 + [\delta_\theta]) \tag{8}$$

Preprints (www.preprints.org) | NOT PEER-REVIEWED | Posted: 17 August 2022 doi:10.20944/preprints202207.0247.v2

Where, $\overline{\theta}$ and $\underline{\theta}$ are the upper and lower limits of parameters respectively. $-\Delta\theta$ and $\Delta\theta_r$ are the left and right extreme values of parameter uncertainty respectively.

For measurement uncertainty:

$$\left[\underline{S_T}, \overline{S_T}\right] = \left[S_M - \Delta S_l, S_M + \Delta S_r\right] = S_M + \left[\xi_S\right] \tag{9}$$

Where, $\overline{S_T}$ and $\underline{S_T}$ are the upper and lower limits of true value respectively. $-\Delta S_l$ and ΔS_r are the left and right extreme values of measurement uncertainty respectively.

Therefore, for pressure variable p, the expanded system level interval analytical redundancy relations is:

$$p = \left[\underline{R}, \overline{R}\right] \cdot \left[\underline{SSQ_T}, \overline{SSQ_T}\right] = R_n SSQ_M + (R_n SSQ_M[\delta_R] + [R_n(1+[\delta_R])] \cdot [-\Delta S_l, \Delta S_r]) \tag{10}$$

At this time, the uncertainty is expanded to $(R_n SSQ_M[\delta_R] + [R_n(1+[\delta_R])] \cdot [-\Delta S_l, \Delta S_r])$. And $R_n SSQ_M$ is the residual term without considering the uncertainty.

After comprehensive consideration of the above uncertainties and negative factors, the diagnostic bond graph of the uncertain landing gear R/E hydraulic system is established, as shown in Figure 12.

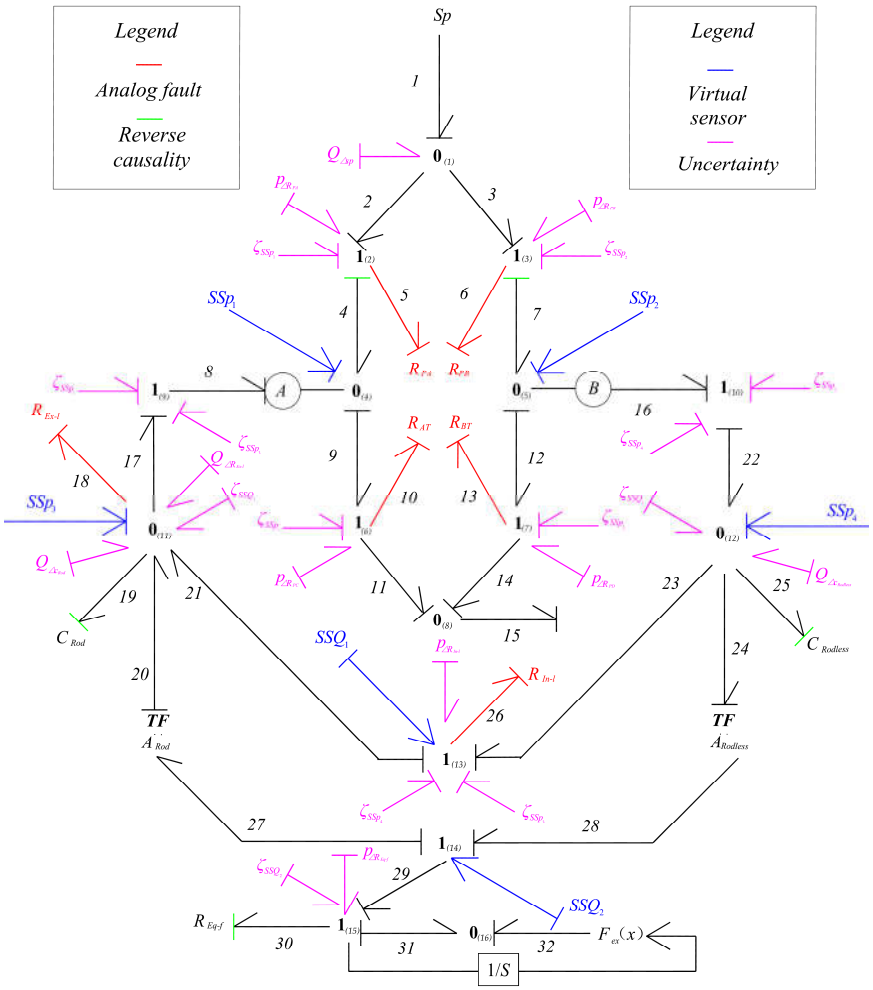

Since there is no such thing as an absolutely perfect system without degradation, the fault-free modeling of the system takes into account a wide variety of potential leaky fluid resistances and stuck fluid resistances, etc. In order to simulate and inject faults, only the pertinent resistive element parameters need to be changed.

There are numerous ways to categorize defects, including minor, general, serious, and deadly faults based on the degree of degradation of faults, and abrupt and

Preprints (www.preprints.org) | NOT PEER-REVIEWED | Posted: 17 August 2022 doi:10.20944/preprints202207.0247.v2

progressive faults based on the degree of progression of faults. A, B, and C are the 3 typical defects examined in this study. Table 3 lists the designed fault types. Define the Boolean logic variable β that will be used to describe the system's operational state:

$$\beta = [\mathrm{A,B,C}] \quad (\mathrm{A/B/C} = 0 \ or \ 1) \tag{11}$$

For example, $\beta = [0,0,1]$ means that only type C fault exist and no type A and B.

Table 3. Fault type and corresponding parameters.

Fault type number	Components involved	Meaning
A	R_{In-l}	Internal leakage of actuator
B	R_{Ex-l}	External leakage of actuator
C	R_{PA} R_{PB} R_{AT} R_{BT}	Landing gear selector valve stuck

ARR at the co-potential node (0-node) can be summarized as " Same potential variable divides the flow variable ", and at the co-flow node (1-node) can be summarized as " Same flow variable divides the potential variable ":

$$0-\mathrm{node}:\begin{cases} p_1 = p_2 = p_3 = \cdots p_n \\ \mathrm{ARR} = \sum_{i=1}^{n} \alpha_i Q_i \end{cases} \quad i = 1,2,3,\cdots n \tag{12}$$

$$1-\mathrm{node}:\begin{cases} Q_1 = Q_2 = Q_3 = \cdots Q_n \\ \mathrm{ARR} = \sum_{i=1}^{n} \alpha_i p_i \end{cases} \quad i = 1,2,3,\cdots n \tag{13}$$

where n is the node's bond excluding the virtual sensor; α_i is the power flow coefficient, for the bond with the half-arrow pointing to the node $\alpha_i = 1$ and for the bond with the half-arrow departing from the node $\alpha_i = -1$.

According to Figure 5, analytical redundancy relations (ARRs) and residuals r_i are obtained.

ARR1 for node $0_{(4)}$:

$$0_{(4)}-\mathrm{node}:\begin{cases} p_4 = p_8 = p_9 \\ \mathrm{ARR}_1 = Q_4 + Q_8 - Q_9 = 0 \end{cases} \tag{14}$$

$$\begin{cases} Q_4 = Q_2 = Q_5 = \dfrac{p_5}{R_{PA}} = \dfrac{p_2 - p_4}{R_{PA}} = \dfrac{Sp - SSp_1}{R_{PA}} \\ Q_8 = Q_{17} = Q_{21} + Q_{20} - Q_{19} - Q_{18} = SSQ_1 + \dfrac{SSQ_2}{A_{Rod}} - C_{Rod}\dfrac{d(SSp_3)}{dt} - \dfrac{SSp_3}{R_{Ex-l}} \\ Q_9 = Q_{10} = Q_{11} = \dfrac{p_{10}}{R_{AT}} = \dfrac{p_9 - p_{11}}{R_{AT}} = \dfrac{SSp_1 - p_T}{R_{AT}} \end{cases} \tag{15}$$

$$r_1 = \frac{Sp - SSp_1}{R_{PA}} + SSQ_1 + \frac{SSQ_2}{A_{Rod}} - C_{Rod}\frac{d(SSp_3)}{dt} - \frac{SSp_3}{R_{Ex-l}} - \frac{SSp_1 - p_T}{R_{AT}} \tag{16}$$

ARR2 for node $0_{(5)}$:

$$0_{(5)}-\mathrm{node}:\begin{cases} p_7 = p_{12} = p_{16} \\ \mathrm{ARR}_2 = Q_7 - Q_{12} - Q_{16} = 0 \end{cases} \tag{17}$$

Preprints (www.preprints.org) | NOT PEER-REVIEWED | Posted: 17 August 2022 doi:10.20944/preprints202207.0247.v2

$$\begin{cases} Q_7 = Q_3 = Q_6 = \dfrac{p_6}{R_{PB}} = \dfrac{p_3 - p_7}{R_{PB}} = \dfrac{Sp - SSp_2}{R_{PB}} \\ Q_{12} = Q_{13} = Q_{14} = \dfrac{p_{13}}{R_{BT}} = \dfrac{p_{12} - p_{14}}{R_{BT}} = \dfrac{SSp_2 - p_T}{R_{BT}} \\ Q_{16} = Q_{22} = Q_{23} + Q_{24} + Q_{25} = SSQ_1 + A_{Rodless} SSQ_2 + C_{Rodless} \dfrac{d(SSp_4)}{dt} \end{cases} \tag{18}$$

$$r_2 = \frac{Sp - SSp_2}{R_{PB}} - \frac{SSp_2 - p_T}{R_{BT}} - SSQ_1 - A_{Rodless} SSQ_2 - C_{Rodless} \frac{d(SSp_4)}{dt} \tag{19}$$

ARR3 for node $1_{(13)}$:

$$1_{(13)} - \text{node:} \begin{cases} Q_{23} = Q_{21} = Q_{26} \\ \text{ARR}_3 = p_{23} - p_{21} - p_{26} = 0 \end{cases} \tag{20}$$

$$\begin{cases} p_{21} = SSp_3 \\ p_{23} = SSp_4 \\ p_{26} = R_{In-l} SSQ_1 \end{cases} \tag{21}$$

$$r_3 = SSp_4 - SSp_3 - R_{In-l} SSQ_1 \tag{22}$$

ARR4 for node $1_{(14)}$:

$$1_{(14)} - \text{node:} \begin{cases} Q_{27} = Q_{28} = Q_{29} \\ \text{ARR}_4 = p_{28} - p_{27} - p_{29} = 0 \end{cases} \tag{23}$$

$$\begin{cases} p_{27} = \dfrac{p_{20}}{A_{Rod}} = \dfrac{SSp_3}{A_{Rod}} \\ p_{28} = A_{Rodless} p_{24} = A_{Rodless} SSp_4 \\ p_{29} = p_{30} + p_{31} = R_{Eq-f} SSQ_2 + F_{ex}(x) \end{cases} \tag{24}$$

$$r_4 = A_{Rodless} SSp_4 - \frac{SSp_3}{A_{Rod}} - R_{Eq-f} SSQ_2 - F_{ex}(x) \tag{25}$$

Define the residual r_i, which has no dimensions of its own. In accordance with the correlation between parameters and ARRs, the fault signature matrix (FSM) is obtained. FSM is shown in Table 4. For the elements M_{mn}, m is the number of rows, n is the number of columns in the matrix, and the relationship is:

$$M_{mn} = \begin{cases} 1 & Parameter \in \text{ARR}_i(r_i) \\ 0 & Parameter \notin \text{ARR}_i(r_i) \end{cases} \tag{26}$$

For any parameter corresponding to a lateral quantity such as $M_{1n} = [M_{11}, M_{12}, M_{13}, \cdots, M_{1n}]$, detectability D_b and isolatability I_b are:

$$D_b = \begin{cases} 1 & M_{1n} = [M_{11}, M_{12}, M_{13}, \cdots, M_{1n}] \neq [0, \cdots, 0] \\ 0 & M_{1n} = [M_{11}, M_{12}, M_{13}, \cdots, M_{1n}] = [0, \cdots, 0] \end{cases} \tag{27}$$

$$I_b = \begin{cases} 1 & M_{1n} = [M_{11}, M_{12}, M_{13}, \cdots, M_{1n}] \text{ is unique} \\ 0 & M_{1n} = [M_{11}, M_{12}, M_{13}, \cdots, M_{1n}] \text{ is not unique} \end{cases} \tag{28}$$

Preprints (www.preprints.org) | NOT PEER-REVIEWED | Posted: 17 August 2022 doi:10.20944/preprints202207.0247.v2

$$\begin{cases} r_i = \mathrm{ARR}_i = 0 & No\ fault \\ r_i = \mathrm{ARR}_i \neq 0 & Faulty \end{cases} \tag{29}$$

When a parameter in the FSM deviates from the nominal value, the detectability indicates that the fault can be detected, but not all parameters are separable. The FSM's non-zero elements have been identified by a distinctive hue that denotes the following:

Red: residual elements in the matrix that are not 0.

Blue: detectability element that is not 0.

Green: isolability element that is not 0.

Table 4. Fault signature matrix of landing gear R/E hydraulic system.

Parameter	r_1	r_2	r_3	r_4	D_b	I_b
Sp	1	1	0	0	1	0
R_{Ex-l}	1	0	0	0	1	0
R_{In-l}	0	0	1	0	1	1
R_{PA}	1	0	0	0	1	0
R_{PB}	0	1	0	0	1	0
R_{AT}	1	0	0	0	1	0
R_{BT}	0	1	0	0	1	0
p_T	1	1	0	0	1	0
C_{Rod}	1	0	0	0	1	0
$C_{Rodless}$	0	1	0	0	1	0
A_{Rod}	1	0	0	1	1	1
$A_{Rodless}$	0	1	0	1	1	1
R_{Eq-f}	0	0	0	1	1	0
$F_{ex}(x)$	0	0	0	1	1	0

4.2. Interval analytical redundancy relations method

Based on the traditional analytical redundancy relation method, the interval analytical redundancy relation method in Section 3 is introduced. According to Figure 12, the residual derivation under the interval analytical redundancy relations is performed.

Taking residual r_1 as an example, the new residual r_1' after considering the negative effects of various uncertainties of the system is

$$\begin{aligned} r_1' = {} & \frac{(1+\delta_{Sp})Sp-(SSp_1+\zeta_{SSp_1})}{(1+\delta_{R_{PA}})R_{PA}}+(SSQ_1+\zeta_{SSQ_1})+\frac{SSQ_2+\zeta_{SSQ_2}}{(1+\delta_{A_{Rod}})A_{Rod}} \\ & -(1+\delta_{C_{Rod}})C_{Rod}\frac{d(SSp_3+\zeta_{SSp_3})}{dt}-\frac{SSp_3+\zeta_{SSp_3}}{(1+\delta_{R_{Ex-l}})R_{Ex-l}}-\frac{(SSp_1+\zeta_{SSp_1})-(1+\delta_{p_T})p_T}{(1+\delta_{R_{AT}})R_{AT}} \end{aligned} \tag{30}$$

Wherein, δ is the corresponding of the parameter, and ζ is the uncertainty of the measured value of the sensor.

After considering the interval analytic redundancy method, r_1' becomes $\left[r_1'\right]$.

Preprints (www.preprints.org) | NOT PEER-REVIEWED | Posted: 17 August 2022 doi:10.20944/preprints202207.0247.v2

$$\begin{aligned}\left[r_1'\right]=\left[\underline{r_1'},\overline{r_1'}\right]&=\frac{(1+\left[\delta_{Sp}\right])Sp-(SSp_1+\left[\zeta_{SSp_1}\right])}{(1+\left[\delta_{R_{PA}}\right])R_{PA}}+(SSQ_1+\left[\zeta_{SSQ_1}\right])+\frac{SSQ_2+\left[\zeta_{SSQ_2}\right]}{(1+\left[\delta_{A_{Rod}}\right])A_{Rod}}\\&-(1+\left[\delta_{C_{Rod}}\right])C_{Rod}\frac{d(SSp_3+\left[\zeta_{SSp_3}\right])}{dt}-\frac{SSp_3+\left[\zeta_{SSp_3}\right]}{(1+\left[\delta_{R_{Ex-l}}\right])R_{Ex-l}}-\frac{(SSp_1+\left[\zeta_{SSp_1}\right])-(1+\left[\delta_{p_T}\right])p_T}{(1+\left[\delta_{R_{AT}}\right])R_{AT}}\end{aligned}\tag{31}$$

$\left[r_2'\right]$, $\left[r_3'\right]$, $\left[r_4'\right]$ can be obtained according to the same method:

$$\begin{cases}\left[r_2'\right]=\left[\underline{r_2'},\overline{r_2'}\right]=\dfrac{(1+\left[\delta_{Sp}\right])Sp-(SSp_2+\left[\zeta_{SSp_2}\right])}{(1+\left[\delta_{R_{PB}}\right])R_{PB}}-\dfrac{(SSp_2+\left[\zeta_{SSp_2}\right])-(1+\left[\delta_{p_T}\right])p_T}{(1+\left[\delta_{R_{BT}}\right])R_{BT}}\\\quad-(SSQ_1+\left[\zeta_{SSQ_1}\right])-(1+\left[\delta_{A_{Rodless}}\right])A_{Rodless}(SSQ_2+\left[\zeta_{SSQ_2}\right])-(1+\left[\delta_{C_{Rodless}}\right])C_{Rodless}\dfrac{d(SSp_4+\left[\zeta_{SSp_4}\right])}{dt}\\\left[r_3'\right]=\left[\underline{r_3'},\overline{r_3'}\right]=(SSp_4+\left[\zeta_{SSp_4}\right])-(SSp_3+\left[\zeta_{SSp_3}\right])-(1+\delta_{R_{In-l}})R_{In-l}(SSQ_1+\left[\zeta_{SSQ_1}\right])\\\left[r_4'\right]=\left[\underline{r_4'},\overline{r_4'}\right]=(1+\left[\delta_{A_{Rodless}}\right])A_{Rodless}(SSp_4+\left[\zeta_{SSp_4}\right])-\dfrac{SSp_3+\left[\zeta_{SSp_3}\right]}{(1+\left[\delta_{A_{Rod}}\right])A_{Rod}}\\\quad-(1+\left[\delta_{R_{Eq-f}}\right])R_{Eq-f}(SSQ_2+\left[\zeta_{SSQ_2}\right])-(1+\left[\delta_{F_{ex}(x)}\right])F_{ex}(x)\end{cases}\tag{32}$$

See Table 5 for interval values in equations (37) and (38).

Table 5. Interval values in equations (37) and (38).

Parameter uncertainty	Measurement uncertainty
$\left[\delta_{Sp}\right]=\left[-\Delta Sp_l/Sp,\Delta Sp_r/Sp\right]$	$\left[\zeta_{SSp_1}\right]=\left[-\Delta SSp_{1_l},\Delta SSp_{1_r}\right]$
$\left[\delta_{R_{PA}}\right]=\left[-\Delta R_{PA_l}/R_{PA},\Delta R_{PA_r}/R_{PA}\right]$	
$\left[\delta_{A_{Rod}}\right]=\left[-\Delta A_{Rod_l}/A_{Rod},\Delta A_{Rod_r}/A_{Rod}\right]$	$\left[\zeta_{SSp_2}\right]=\left[-\Delta SSp_{2_l},\Delta SSp_{2_r}\right]$
$\left[\delta_{C_{Rod}}\right]=\left[-\Delta C_{Rod_l}/C_{Rod},\Delta C_{Rod_r}/C_{Rod}\right]$	
$\left[\delta_{R_{Ex-l}}\right]=\left[-\Delta R_{Ex-l_l}/R_{Ex-l},\Delta R_{Ex-l_r}/R_{Ex-l}\right]$	$\left[\zeta_{SSp_3}\right]=\left[-\Delta SSp_{3_l},\Delta SSp_{3_r}\right]$
$\left[\delta_{R_{AT}}\right]=\left[-\Delta R_{AT_l}/R_{AT},\Delta R_{AT_r}/R_{AT}\right]$	
$\left[\delta_{p_T}\right]=\left[-\Delta p_{T_l}/p_T,\Delta p_{T_r}/p_T\right]$	$\left[\zeta_{SSp_4}\right]=\left[-\Delta SSp_{4_l},\Delta SSp_{4_r}\right]$
$\left[\delta_{R_{In-l}}\right]=\left[-\Delta R_{In-l_l}/R_{In-l},\Delta R_{In-l_r}/R_{In-l}\right]$	
$\left[\delta_{R_{PB}}\right]=\left[-\Delta R_{PB_l}/R_{PB},\Delta R_{PB_r}/R_{PB}\right]$	$\left[\zeta_{SSQ_1}\right]=\left[-\Delta SSQ_{1_l},\Delta SSQ_{1_r}\right]$
$\left[\delta_{R_{BT}}\right]=\left[-\Delta R_{BT_l}/R_{BT},\Delta R_{BT_r}/R_{BT}\right]$	
$\left[\delta_{C_{Rodless}}\right]=\left[-\Delta C_{Rodless_l}/C_{Rodless},\Delta C_{Rodless_r}/C_{Rodless}\right]$	$\left[\zeta_{SSQ_2}\right]=\left[-\Delta SSQ_{2_l},\Delta SSQ_{2_r}\right]$
$\left[\delta_{A_{Rodless}}\right]=\left[-\Delta A_{Rodless_l}/A_{Rodless},\Delta A_{Rodless_r}/A_{Rodless}\right]$	
$\left[\delta_{R_{Eq-f}}\right]=\left[-\Delta R_{Eq-f_l}/R_{Eq-f},\Delta R_{Eq-f_r}/R_{Eq-f}\right]$	
$\left[\delta_{F_{ex}(x)}\right]=\left[-\Delta F_{ex}(x)_l/F_{ex}(x),\Delta F_{ex}(x)_r/F_{ex}(x)\right]$	

There are differential terms $d(SSp_3+\left[\zeta_{SSp_3}\right])/dt$ and $d(SSp_4+\left[\zeta_{SSp_4}\right])/dt$ in equations (37) and (38), respectively. It is necessary to further calculate the first-order differential and the second-order differential by the backward differential method.

Preprints (www.preprints.org) | NOT PEER-REVIEWED | Posted: 17 August 2022 doi:10.20944/preprints202207.0247.v2

$$\begin{cases} \dfrac{d(SSp_3+[\zeta_{SSp_3}])}{dt}=\dfrac{d(SSp_3)}{dt}+[\zeta_{SSp_3}] \\ \dfrac{d(SSp_4+[\zeta_{SSp_4}])}{dt}=\dfrac{d(SSp_4)}{dt}+[\zeta_{SSp_4}] \end{cases} \quad \begin{cases} \dfrac{d^2(SSp_3+[\zeta_{SSp_3}])}{dt^2}=\dfrac{d^2(SSp_3)}{dt^2}+[\zeta_{SSp_3}] \\ \dfrac{d^2(SSp_4+[\zeta_{SSp_4}])}{dt^2}=\dfrac{d^2(SSp_4)}{dt^2}+[\zeta_{SSp_4}] \end{cases} \tag{33}$$

Therefore, the uncertainty terms $[u_1]$, $[u_2]$, $[u_3]$, $[u_4]$ corresponding to $[r_1']$, $[r_2']$, $[r_3']$, $[r_4']$ can be obtained.

$$\begin{cases} [u_1]=\dfrac{(1+[\delta_{Sp}])Sp-(SSp_1+[\zeta_{SSp_1}])}{(1+[\delta_{R_{PA}}])R_{PA}}+[\zeta_{SSQ_1}]+\dfrac{SSQ_2+[\zeta_{SSQ_2}]}{(1+[\delta_{A_{Rod}}])A_{Rod}} \\ \quad -(1+[\delta_{C_{Rod}}])C_{Rod}[\zeta_{SSp_3}]-\dfrac{SSp_3+[\zeta_{SSp_3}]}{(1+[\delta_{R_{Ex-l}}])R_{Ex-l}}-\dfrac{(SSp_1+[\zeta_{SSp_1}])-(1+[\delta_{p_T}])p_T}{(1+[\delta_{R_{AT}}])R_{AT}} \\ [u_2]=\dfrac{(1+[\delta_{Sp}])Sp-(SSp_2+[\zeta_{SSp_2}])}{(1+[\delta_{R_{PB}}])R_{PB}}-\dfrac{(SSp_2+[\zeta_{SSp_2}])-(1+[\delta_{p_T}])p_T}{(1+[\delta_{R_{BT}}])R_{BT}} \\ \quad -[\zeta_{SSQ_1}]-(1+[\delta_{A_{Rodless}}])A_{Rodless}(SSQ_2+[\zeta_{SSQ_2}])-(1+[\delta_{C_{Rodless}}])C_{Rodless}[\zeta_{SSp_4}] \\ [u_3]=[\zeta_{SSp_4}]-[\zeta_{SSp_3}]-\delta_{R_{In-l}}](SSQ_1+[\zeta_{SSQ_1}])-R_{In-l}[\zeta_{SSQ_1}]) \\ [u_4]=[\delta_{A_{Rodless}}]A_{Rodless}(SSp_4+[\zeta_{SSp_4}])+A_{Rodless}[\zeta_{SSp_4}]-\dfrac{SSp_3+[\zeta_{SSp_3}]}{(1+[\delta_{A_{Rod}}])A_{Rod}} \\ \quad -[\delta_{R_{Eq-f}}]R_{Eq-f}(SSQ_2+[\zeta_{SSQ_2}])-R_{Eq-f}[\zeta_{SSQ_2}]-[\delta_{F_{ex}(x)}]F_{ex}(x) \end{cases} \tag{34}$$

4.3. Diagnostic thresholds and data acquisition

Positive, negative, or 0 residuals are possible. It has no dimensions and no physical significance. According to the literature [38,39], threshold deviation is defined as ε_i, and the absolute value type threshold is:

$$\begin{cases} Upper\ threshold = r_i+\varepsilon_i \\ Lower\ threshold = r_i-\varepsilon_i \end{cases} \tag{35}$$

After considering the negative factors such as uncertainty $\varepsilon_i=\Delta\theta_i|u_{\theta_i}|$, the absolute value type diagnostic threshold is:

$$\begin{cases} Upper\ threshold = r_i+\Delta\theta_i|u_{\theta_i}| \\ Lower\ threshold = r_i-\Delta\theta_i|u_{\theta_i}| \end{cases} \tag{36}$$

The defined uncertainty value is shown in Table 6, and the uncertainty measure is 1% of the original value. And the measurement uncertainty error is defined as 0.1%.

According to the diagnostic bond graph in Figure 12, as illustrated in Figure 13, the diagnostic simulation model is created in the LMS Imagine.Lab AMESim simulation platform. On the diagnostic bond graph, the sensor shown in the illustration is the same sensor.

The premise of the model-based simulation experiment is to prove the validity of the model. According to the professional maintenance manuals of Boeing and Airbus [40-42], as well as the computer-based training videos of maintenance professionals, under normal circumstances, the retraction time of landing gear is 7.5s and the extension time is 10s, which may vary slightly with different aircraft types.

Actuator action is opposite to landing gear body action. When the retraction/extension actuator is extended, the landing gear retracts; When the actuator is retracted, the

Preprints (www.preprints.org) | NOT PEER-REVIEWED | Posted: 17 August 2022 doi:10.20944/preprints202207.0247.v2

landing gear is retracted. The results of the diagnostic simulation model are shown in Figure 14. The retraction time of the actuator is from 2s to 12.86s, and the extension time of the actuator is from 2s to 9.17s.

Introducing [43] sum of squares of errors (SSE), mean-squared error (MSE), and model effect evaluation index R^2.

$$\begin{cases} SSE=\sum_{i=1}^{n}(y_i-\hat{y}_i)^2 \\ MSE=\sqrt{\frac{1}{n}\sum_{i=1}^{n}(y_i-\hat{y}_i)^2} \\ R^2=\frac{SSE-MSE}{SSE} \end{cases} \tag{37}$$

Where y_i and $\hat{y}_i$ are the expected value and the actual value, respectively. MSE is the error that cannot be explained by the model, so the larger R^2 is, the better.

According to the model matching evaluation method, the R^2 is 0.7676. Therefore, the evaluation effect of this model is favorable.

Table 6. The defined uncertainty value.

Parameter	Nominal value	Absolute value type uncertainty	Interval type uncertainty
Sp	$2.0685\times10^7\,Pa(3000\,psi)$	$\pm2.0685\times10^5$	$[-1.2000\times10^5, 2.0685\times10^5]$
R_{Ex-l}	$9.35\times10^6\,N\cdot s/m^5$	$\pm9.35\times10^4$	$[-7.50\times10^4, 9.35\times10^4]$
R_{In-l}	$3.40\times10^6\,N\cdot s/m^5$	$\pm3.40\times10^4$	$[-1.80\times10^4, 3.40\times10^4]$
R_{PA}	$2.0\times10^{12}\,N\cdot s/m^5$	$\pm2.0\times10^{10}$	$[-0.5\times10^{10}, 2.0\times10^{10}]$
R_{PB}	$2.0\times10^{12}\,N\cdot s/m^5$	$\pm2.0\times10^{10}$	$[-0.5\times10^{10}, 2.0\times10^{10}]$
R_{AT}	$7.8\times10^9\,N\cdot s/m^5$	$\pm7.8\times10^7$	$[-5.0\times10^7, 7.8\times10^7]$
R_{BT}	$7.8\times10^9\,N\cdot s/m^5$	$\pm7.8\times10^7$	$[-5.0\times10^7, 7.8\times10^7]$
p_T	$2500Pa$	±25	$[-5, 25]$
C_{Rod}	$8.30\times10^{-13}\,m^5/N$	$\pm8.30\times10^{-15}$	$[-3.60\times10^{-15}, 8.30\times10^{-15}]$
$C_{Rodless}$	$2.55\times10^{-13}\,m^5/N$	$\pm2.55\times10^{-15}$	$[-1.50\times10^{-15}, 2.55\times10^{-15}]$
A_{Rod}	$0.0075m^2$	$\pm7.50\times10^{-5}$	$[-4.50\times10^{-5}, 7.50\times10^{-5}]$
$A_{Rodless}$	$0.0125m^2$	$\pm1.25\times10^{-4}$	$[-0.50\times10^{-4}, 1.25\times10^{-4}]$
R_{Eq-f}	$5.5\times10^{14}\,N\cdot s/m^5$	$\pm5.5\times10^{12}$	$[-3.0\times10^{12}, 5.5\times10^{12}]$
$F_{ex}(x)$	$2.22\times10^5\,Pa$	$\pm2.22\times10^3$	$[-1.00\times10^3, 2.22\times10^3]$

Preprints (www.preprints.org) | NOT PEER-REVIEWED | Posted: 17 August 2022 doi:10.20944/preprints202207.0247.v2

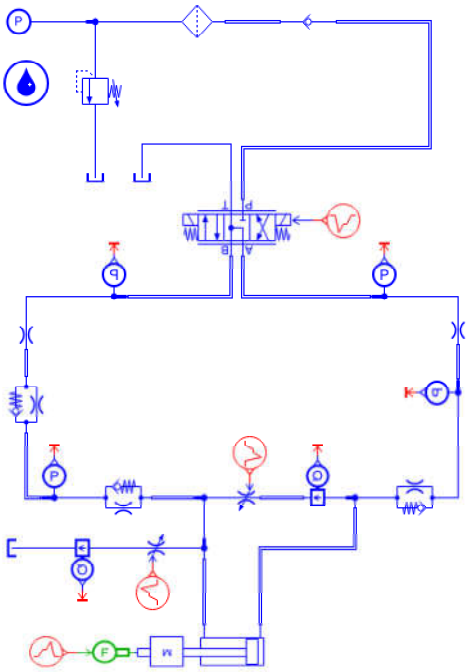

Figure 13. Diagnostic simulation model of the system.

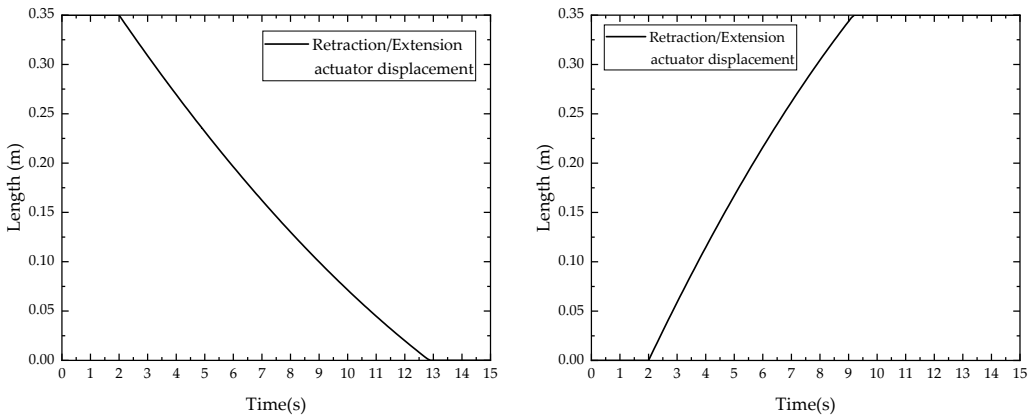

Figure 14. Simulation result of diagnostic model: (**a**) Actuator retraction; (**b**) Actuator extension.

5. Fault case analysis

5.1. Fault free operation of the system

The above output data is analyzed by the INTLAB interval operation toolkit under MATLAB. Its operation rules can be seen in [44]. The residuals $\left[r_1'\right]$, $\left[r_2'\right]$, $\left[r_3'\right]$, $\left[r_4'\right]$ under fault free operation are shown in Figure 15, wherein the diagnosis thresholds are of absolute type (AT) and interval type (IT) respectively.

In general, the continuous deterioration of the residual will continue to extend in either the positive direction or the negative direction. In the process of deterioration, it will not suddenly change from a positive value to a negative value at a certain time, and vice versa. Therefore, the trend of the residual can be understood through trial test. On the basis of the diagnostic threshold method proposed above, the threshold can be appropriately reduced in the direction of the residual to further improve the diagnostic sensitivity.

Preprints (www.preprints.org) | NOT PEER-REVIEWED | Posted: 17 August 2022 doi:10.20944/preprints202207.0247.v2

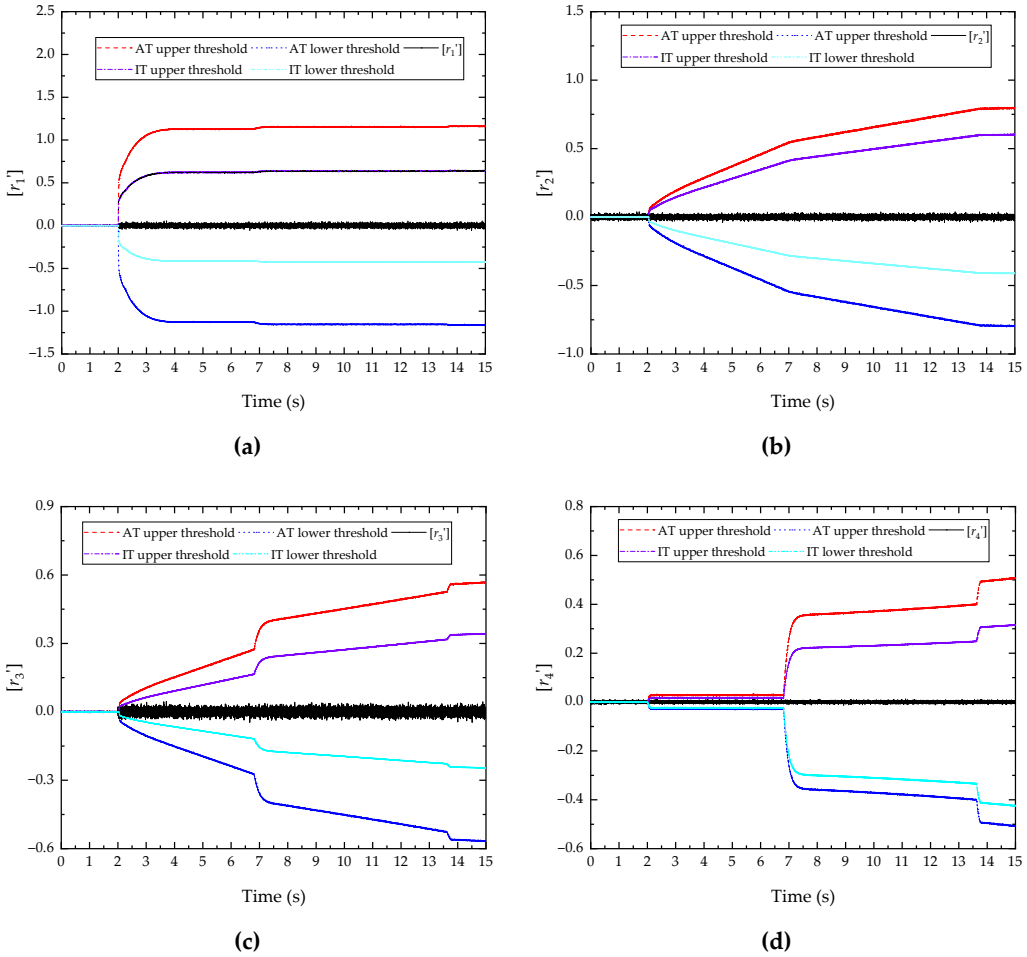

Figure 15. Fault free system operation fault detection results: (**a**) $\left[r_1'\right]$ (**b**) $\left[r_2'\right]$; (**c**) $\left[r_3'\right]$; (**d**) $\left[r_4'\right]$.

It can be seen from Figure 15 that the residuals $\left[r_1'\right]$, $\left[r_2'\right]$, $\left[r_3'\right]$ and $\left[r_4'\right]$ fluctuate up and down within a certain range of 0, and all do not exceed the diagnostic threshold. This indicates that no fault is detected during normal operation of the system, corresponding to $\beta=[0,0,0]$. Therefore, it can be proved that the uncertainty interference modeling and analysis method proposed in this paper is correct and feasible.

5.2. External and internal leakage of actuator

One of the actuator's most prevalent failure types is leakage, as shown by the fundamental ideas in Figure 16. There is no escape from it; it is an inherent mode. Generally, it is controlled by increasing tightness and performing regular inspections [45,46]. Figure 16 shows the leakage flow, which is represented by the red dotted line. There are two types of leaks: internal and external. Internal leaks happen between the cylinder and piston, while external leaks happen between the piston rod and cylinder. Take the piston rod extension as an example. When high-pressure hydraulic oil forces the piston out of the actuator cylinder, flow loss will occur between these two kinds of gaps.

Preprints (www.preprints.org) | NOT PEER-REVIEWED | Posted: 17 August 2022 doi:10.20944/preprints202207.0247.v2

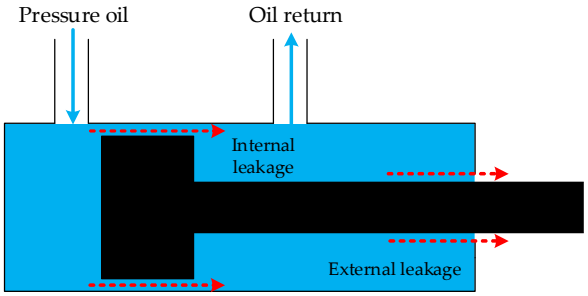

Figure 16. Basic principle of actuator leakage.

External leakage and internal leakage of the actuating cylinder are a pair of simultaneous failure modes. To simulate the leakage fault of the actuator, set the external leakage parameter R_{Ex-l} and internal leakage parameter R_{In-l} in Table 4 and 5 to meet the following relationship:

$$\begin{cases} R_{Ex-l} = 9.35\times10^{6}\cdot\left[1+0.08(t-2)\right] & 2\le t\le 15 \\ R_{In-l} = 3.40\times10^{6}\cdot\left[1+0.05(t-2)\right] & 2\le t\le 15 \end{cases} \tag{38}$$

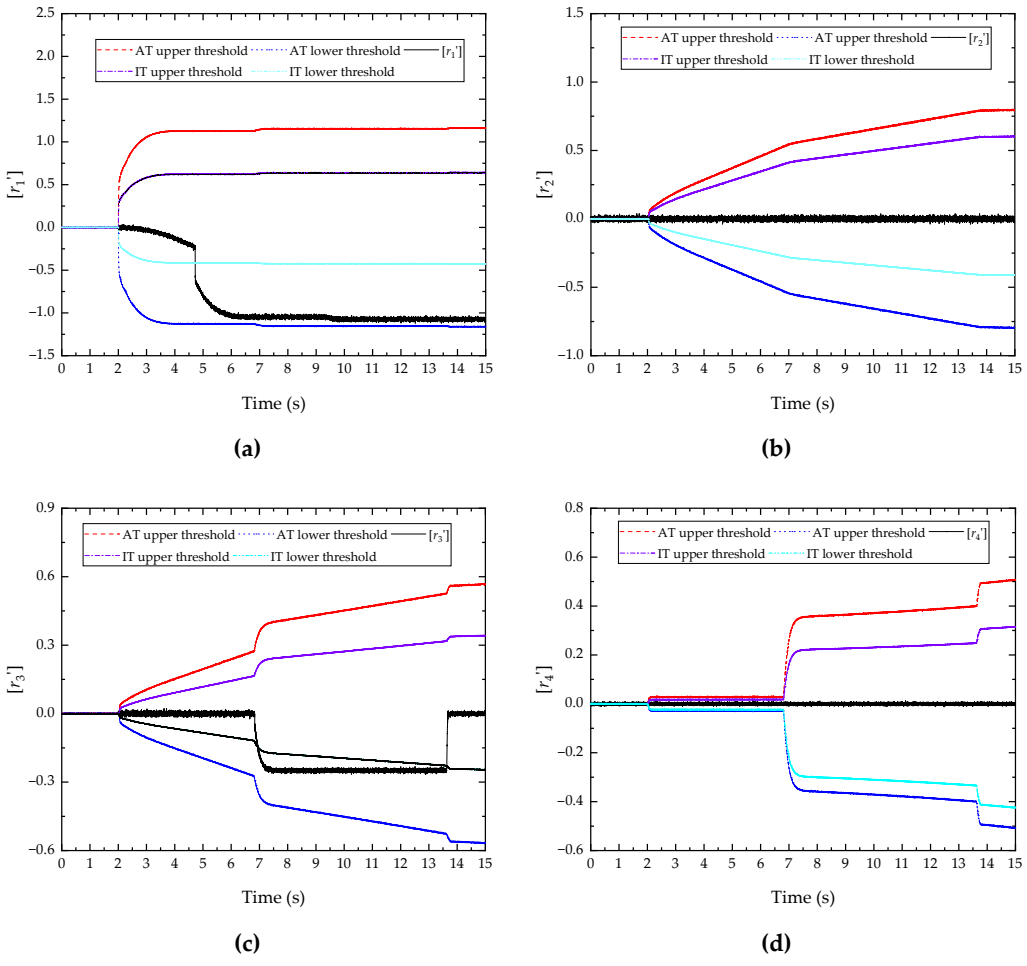

Figure 17. External and internal leakage of actuator fault detection results: (**a**) $\left[r_1'\right]$ (**b**) $\left[r_2'\right]$; (**c**) $\left[r_3'\right]$; (**d**) $\left[r_4'\right]$.

Preprints (www.preprints.org) | NOT PEER-REVIEWED | Posted: 17 August 2022 doi:10.20944/preprints202207.0247.v2

Figure 17 (a) shows that the residual $\left[r_1'\right]$ exceeds the interval type (IT) lower threshold at 4.83s, and external leakage of actuator cylinder is successfully diagnosed. However, the residual $\left[r_1'\right]$ does not exceed the absolute type (AT) lower threshold not tested, resulting in missed diagnosis.

Figure 17 (c) shows that the residual $\left[r_3'\right]$ exceeds the interval type (IT) lower threshold at 7.05s, and internal leakage of actuator cylinder is successfully diagnosed. However, the residual $\left[r_3'\right]$ does not exceed the absolute type (AT) lower threshold not tested, resulting in missed diagnosis.

The residuals $\left[r_2'\right]$ and $\left[r_4'\right]$ in Figure 17 (b) and (d) are basically no different from the normal operation of the system, which proves that the two threshold methods do not cause misdiagnosis. This also corresponds to β=[1,1,0].

5.3. Landing gear selector valve reversing stuck

Landing gear selector valve has 3 operational states [47]: Neutral, Left, and Right. Using the left as an example, we can see from the analysis above that at this moment, we do not take the liquid resistance R_{PA} and R_{BT} into consideration, they are constant fixed values, the fault diagnosis object is the liquid resistance R_{PB} and R_{AT}. R_{PB} corresponds to $\left[r_2'\right]$, R_{AT} corresponds to $\left[r_1'\right]$. Shifting to the right reverses the object of research and control invariant liquid resistance. Set the liquid resistance R_{PB} and R_{AT} in Table 4 and 5 to meet the following relationship:

$$\begin{cases} R_{PB} = 2.0\times10^{12}\cdot\left[1+0.35(t-2)\right] & 2\le t\le 15 \\ R_{AT} = 7.8\times10^{9}\cdot\left[1+0.20(t-2)\right] & 2\le t\le 15 \end{cases} \tag{39}$$

Figure 18 (a) shows that the residual $\left[r_1'\right]$ exceeds the interval type (IT) lower threshold at 3.50s and the absolute type (AT) lower threshold at 5.92s. Both of them successfully detect the preset fault, but the AT has better sensitivity.

Figure 18 (b) shows that the residual $\left[r_2'\right]$ exceeds the interval type (IT) lower threshold at 4.42s, and landing gear selector valve reversing stuck is successfully diagnosed. However, the residual $\left[r_2'\right]$ does not exceed the absolute type (AT) lower threshold not tested, resulting in missed diagnosis.

The residuals $\left[r_3'\right]$ and $\left[r_4'\right]$ in Figure 18 (b) and (d) are basically no different from the normal operation of the system, which proves that the two threshold methods do not cause misdiagnosis. This also corresponds to β=[0,0,1].

Preprints (www.preprints.org) | NOT PEER-REVIEWED | Posted: 17 August 2022 doi:10.20944/preprints202207.0247.v2

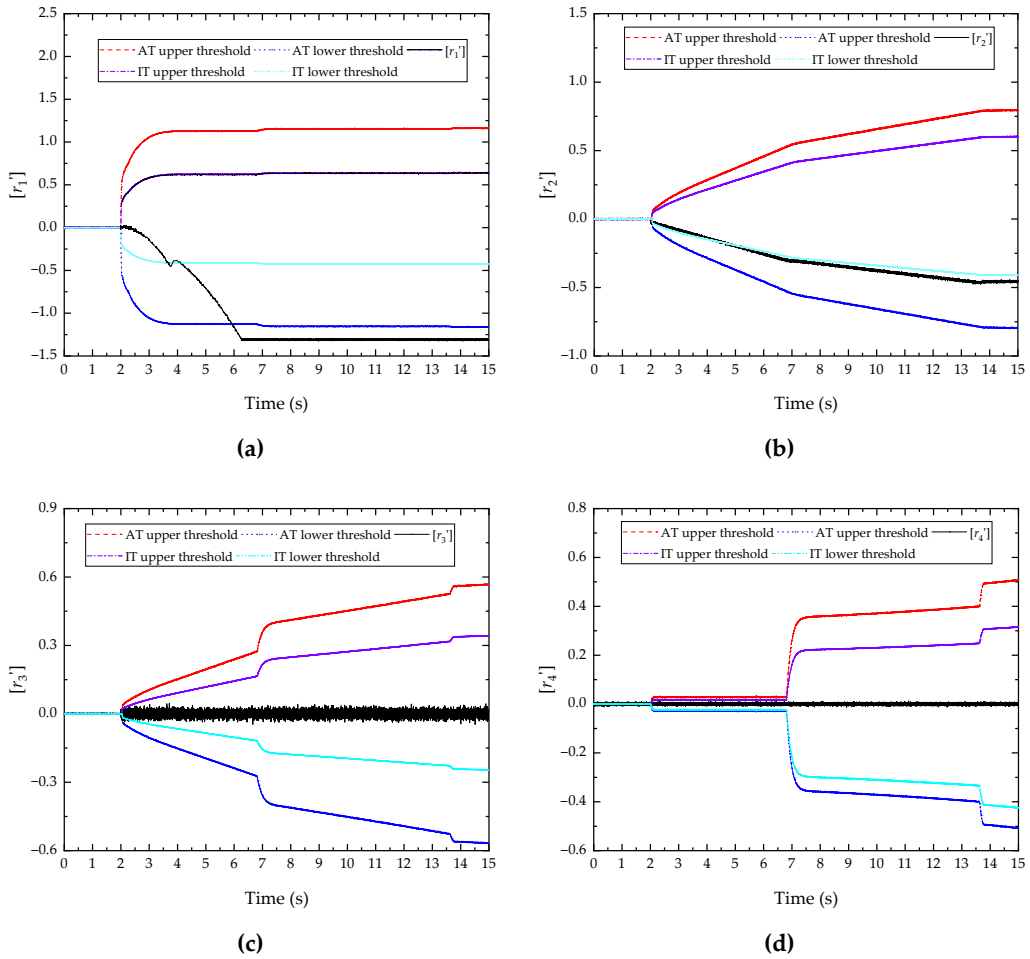

Figure 18. Fault free system operation fault detection results: (**a**) $\left[r_1'\right]$ (**b**) $\left[r_2'\right]$; (**c**) $\left[r_3'\right]$; (**d**) $\left[r_4'\right]$.

6. Conclusions

Landing gear retraction/extension hydraulic system is a nonlinear dynamic system. Without considering the uncertainty of component parameters and sensor measurement values in fault diagnosis research, missed diagnoses and misdiagnoses are likely to occur. In order to model the uncertainty diagnosis of the landing gear retraction/extension hydraulic system, bond graph linear fractional transformation technology and interval analytical redundancy relations are used. According to case analysis, the diagnosis method proposed in this paper has higher detection accuracy and sensitivity than both the method without considering interference factors and the traditional absolute value threshold analysis. Nevertheless, this paper only isolates a preliminary fault based on the fault signature matrix, and further research is required.

Author Contributions: Manuscript Writing, Y.C. and S.D.; manuscript Revision, Y.L.; simulation test: S.D. and X.L.; project Funding: Y.C.; reference and data collation: Z.Z. and X.W. All authors have read and agreed to the published version of the manuscript.

Funding: This research was funded by [the Aero-Science Fund of China] grant number [20200033052001] and [Nanjing University of Aeronautics and Astronautics Postgraduate Innovation Base Open Fund] grant number [kfjj20200725].

Conflicts of Interest: The authors declare no conflict of interest.

References

1. *Boeing, Statistical Summary of Commercial Jet Airplane Accidents Worldwide Operations 1959–2017*; 2017.
2. *Airbus, A Statistical Analysis of Commercial Aviation Accidents 1958-2018*; 2018.
3. *EASA, Annual Safety Review 2020*; 2020.
4. *ICAO, State of Global Aviation Safety;* 2019.
5. Han, X. Research on Lightweight Distributed Neural Network Technology for Fault Diagnosis. Master's Thesis, Zhejiang University, Hangzhou, China, **2022**.
6. Yang, Y. Aircraft landing gear extension and retraction control system diagnostics prognostics and health management. Master's Thesis, Cranfield University, London, UK, **2012**.
7. Shao, W. Research on the FMECA and FTA of the Landing Gear System for A Certain Type of Aircraft in Failure Analysis. Master's Thesis, Xihua University, Chengdu, China, **2019**.
8. Ji, X. Simulation and Research on Electrical Characteristics of Retraction and Extension Faults of More Electric Aircraft's Landing Gear. Master's Thesis, Civil Aviation University of China, Tianjin, China, **2019**.
9. Juan, J; Roque, A; Rene, D. Industrial Data-Driven Monitoring Based on Incremental Learning Applied to the Detection of Novel Faults. *IEEE Transactions on Industrial Informatics*. **2020**, 16, 5985-5995.
10. Prasad, D; Nayak, K. Performance assessment of swarm-assisted mean error estimation-based fault detection technique for transmission line protection. *Computers and Electrical Engineering*. **2018**, 71, 115-128.
11. Sara, N; Mohammad, R; Kerstin, W. Fracture mechanics and mechanical fault detection by artificial intelligence methods: A review. *Engineering Failure Analysis*. **2017**, 81, 270-293.
12. Li, F; Wu, Z; Li, J; Lai, Z; Zhao, B; Min, C. A Multi-Step CNN-Based Estimation of Aircraft Landing Gear Angles. *Sensors.* **2021**, 21, 8440.
13. Chen, J; Xu, Q; Guo, Y; Chen, R. Aircraft Landing Gear Retraction/Extension System Fault Diagnosis with 1-D Dilated Convolutional Neural Network. *Sensors.* **2022**, 22, 1367.
14. Hu, Z; Zhao, G; Li, F; Zhou, D. Fault diagnosis for nonlinear dynamical system based on adaptive unknown input observer. *Control and Decision.* **2016**, 31, 901-906.
15. Liu, Y; Sun, C; Chen, Y; Lin, G. Design and application on sliding mode controller for roller microporous system based on disturbance observer. *Forging & Stamping Technology*. **2022**, 47, 116-120.
16. Xu, G; Yu, Z; Lu, N; Lv, G. High-gain observer-based sliding mode control for hydraulic excavators. *Journal of Harbin Engineering University*. **2021**, 42, 885-892.
17. Yu, Y; Xiao, Y; Zhu, C; Tong, J. Sliding Mode Control of Crane Anti-sway Positioning Based on Kalman Filter. *Control Engineering of China*. **2021**, 28, 1049-1054.
18. Huang, Y; Bai, M; Zhang, Y. A novel multiple-outlier-robust Kalman filter. *Frontiers of Information Technology & Electronic Engineering*. **2022**, 23, 422-437.
19. Cui, Z; Jing, B; Jiao, X; Yao, W; Zhou, Y. Design of fault-tolerant integrated navigation system based on federated Kalman filter. *Journal of electronic measurement and instrumentation*. **2021**, 35, 143-153.
20. Wang, S. Research on Dynamic State Estimation of Power System Eased on Kalman Filter. Master's Thesis, North China Electric Power University, Beijing, China, 2020.
21. Gao, S; Li, R; Huang, Z. A Fault-tolerance Estimating Method for Ionosphere Corrections in Satellite Navigation System. *Chinese Journal of Aeronautics*. **2011**, 24, 749-755.
22. Shen, W; Yuan, X; Liu, M. Event-triggered Control for Hydraulic Position Tracking System with Extended State Observer. *Journal of Mechanical Engineering*. **2022**, 58, 274-284.
23. Qin, D; Jian, J; Cheng, K, Wu B. Adaptive Starting Control of Dual Clutch Transmission Based on Extended State Observer and Sliding-mode Control. *China Journal of Highway and Transport*. **2021**, 34, 39-50.
24. Najmeh, D; Nader, M; Khashayar, K. A Dual Particle Filter-Based Fault Diagnosis Scheme for Nonlinear Systems. *IEEE Transactions on Control Systems Technology.* **2018**, 26, 1317-1334.
25. Tian, K. Research on the Technology of Prediction and Diagnosis of Equipment Fault in Satellite Ground Station System. Master's Thesis, University of Electronic Science And Technology Of China, Chengdu, China, 2021.
26. Mo, H; Li, Y. Fault Diagnosis Based on Interval Analytic Redundancy Relation. *Journal of Nanjing University of Aeronautics & Astronautics.* **2021**, 53, 972-980.
27. Wang, F; Pazilai, M; Zhang, B. Robust fault diagnosis and fault tolerant control based on bond graph. *Electrical Measurement & Instrumentation*. **2019**, 56, 124-128.
28. Djeziri, M; Bouamama, B; Merzouki, R. Modelling and robust FDI of steam generator using uncertain bond graph model. *Journal of Process Control.* **2009**, 19, 149-162.
29. Duan, S; Li, Y; Cao, Y; Wang, X; Li, X; Zhao, Z. Health Assessment of Landing Gear Retraction/Extension Hydraulic System Based on Improved Risk Coefficient and FCE Model. *Appl. Sci.* **2022**, 12, 5409.
30. Wang, Z. *Bond graph theory and its application in system dynamics*; Harbin Engineering University Press: Harbin, China, **2000**; 38–46.
31. Yin, Y. Dynamics and Reliability Analysis of Retraction of Landing Gear. Doctor's Thesis, Nanjing University of Aeronautics and Astronautics, Nanjing, China, **2017**.

32. Yin, Y; Nie, H; Wei, X; Ni, H. Performance analysis of landing gear retraction and extension system under the influence of multiple factors. *Journal of Beijing University of Aeronautics and Astronautics*. **2015**, 41, 953-960.
33. Medjaher, K; Samantaray, A; Bouamama, O. Diagnostic Bond Graphs for Direct Residual Evaluation. International Conference on Bond Graph Modeling and Simulation (ICBGM'05), New Orleans, Louisiana, U.S.A, 23-26 Jan.2005.
34. Guo, H. Research on fault diagnosis for dissimilar redundant actuation system of more electric aircraft. Master's Thesis, Hefei University of Technology, Hefei, China, 2021.
35. Gao, C. Research on Performance Uncertainty Analysis Methods for Distributed Satellite System in Conceptual Design Phase. Doctor's Thesis, University of Chinese Academy of Sciences, Beijing, China, **2020**.
36. Touati, Y; Merzouki, R; Bouamama, B. Robust diagnosis to measurement uncertainties using bond graph approach: Application to intelligent autonomous vehicle. *Mechatronics*. **2012**, 22, 1148-1160.
37. Sia, K; Namaane, A; M'Sirdi, N. A new structural approach for ARRs generation from linear & linearized bond graphs. 2011 International Conference on Communications, Computing and Control Applications (CCCA), 3-5 Mar.2011
38. Wang, X; Wei, S; Wang, P; Song, X; Li, W. Fault Diagnosis Simulation Method for Luffing Hydraulic System of Truck-mounted *Crane. Chinese Hydraulics & Pneumatics*. **2022**, 46, 173-181.
39. Dutta, S; Kumar, S; Saha, T; Ghoshal, S. Determination of the Degradation Pattern of Pump Using Two-Phase Diagnostic Bond Graph. Lecture Notes in Mechanical Engineering of Springer, Recent Advances in Mechanical Engineering Select Proceedings of NCAME 2019.
40. Boeing, B737-600/700/800/900 Aircraft Maintenance Manual; Aero Ground Training: Ploudaniel, France, 2010.
41. Airbus, A318/A319/A320/A321 Aircraft Maintenance Manual; 2012.
42. *Air Transport Association of America. ATA 100 specification for manufacturers'technical data.* U.S.A, 1999.
43. Holmes, G; Sartor, P; Reed, S; Southern, P; Worden, K; Cross, E. Prediction of Landing Gear Loads Using Machine Learning Techniques. *Structural health monitoring*. **2016**, 15, 578-592.
44. Moore, R; Kearfott, R; Cloud, M. *Introduction to Interval Analysis. Society for Industrial and Applied Mathematics*; Society for Industrial and Applied Mathematics Philadelphia: Philadelphia, U.S.A, **2009**; 37-49**.**
45. Zhou, J; Li, X. Design of a high precision automatic diagnosis method for hydraulic cylinder leakage fault. *Manufacturing Automation.* **2022**, 44, 182-186.
46. Song, F; Chen, J; Peng, L, Liu, J. Experimental research on the internal leakage of hydraulic slide valve. Fluid Machinery. 2021, 49, 1-6+28.
47. Wei, S. Research on Fault Diagnosis Research Method for Luffing Hydraulic System of Lorry-Mounted Crane. Master's Thesis, Dalian University of Technology, Dalian, China, 2021.